Molecular simulation of multi-component adsorption processes related to carbon capture in a high surface area, disordered activated carbon

CARBON 94 (2015) 27–40

Contents lists available at ScienceDirect

CARBON

journal homepage: www.elsevier.com/locate/carbon

Molecular simulation of multi-component adsorption processes related to carbon capture in a high surface area, disordered activated carbon

Emanuela Di Biase, Lev Sarkisov *

Institute for Materials and Processes, School of Engineering, The University of Edinburgh, EH9 3JL, UK

ARTICLE INFO

Article history:
Received 16 April 2015
Received in revised form 17 June 2015
Accepted 18 June 2015
Available online 23 June 2015

ABSTRACT

We employ a previously developed model of a high surface area activated carbon, based on a random packing of small fragments of a carbon sheet, functionalized with hydroxyl surface groups, to explore adsorption of water and multicomponent mixtures under conditions representing typical carbon capture processes. Adsorption of water is initialized and proceeds through the growth of clusters around the surface groups, in a process predominantly governed by hydrogen bond interactions. In contrast, energetically favorable locations for carbon dioxide molecules are different from that for water, with the main contribution coming from the Lennard-Jones interactions with the extended surfaces of the fragments. This explains why over a broad range of conditions small amounts of water do not have any substantial impact on adsorption of carbon dioxide and other species in activated carbons. From the studies of various carbon capture processes, the model material shows promising properties for pre-combustion capture due to large capacity at high pressures and other favorable characteristics.

1. Introduction

Physical adsorption in porous materials is considered as a promising, energy efficient technology for carbon dioxide capture from industrial and energy-related sources [1–3]. Important requirements for materials to be used as adsorbents in this context are good affinity, selectivity and capacity for carbon dioxide, ease of regeneration, stability with respect to components and contaminants in the streams, stability under the conditions of the carbon capture processes, and affordable cost [4–10].

Broadly, there are three different types of CO_2 capture processes that could possibly be applied to fossil-fuel power plants: post-combustion capture, pre-combustion capture and oxyfuel combustion process [11]. Various features of these processes, including conditions, energy requirements, stream compositions, as well as comparative advantages and disadvantages, have been comprehensively reviewed in the literature [1–4,6]. In this article we focus on pre- and post-combustion capture and we also explore the process of sweetening of sour natural gas which, although not directly related to power plant operation, is still associated with carbon capture [6].

As these processes vary substantially in the conditions and composition of the streams to be treated, clearly no single adsorbent material is likely to be suitable in all these processes, and different adsorbents (or a combination of adsorbents) should be considered and optimized in application to a specific separation process [5]. A number of materials, including zeolites, polymers, metal–organic and covalent organic frameworks, metal oxides, carbonaceous sorbents etc. have been explored in the context of carbon capture processes [4–6,9,10,12].

Several publications present advantages and disadvantages associated with the use of activated carbons in the context of carbon dioxide adsorption [5,6,13–16]. In general, activated carbons do not exhibit particularly strong selectivity toward carbon dioxide. As a result, they are unlikely to be used in post-combustion capture, which deals with low partial pressure of carbon dioxide in the stream. Nevertheless, compared to other materials, activated carbons present several advantages. Indeed, they are a very versatile and diverse family of materials, they are commercially available and relatively inexpensive, and they are stable under a broad range of conditions, with highly reproducible and consistent adsorption behavior [17].

In particular, because of their high adsorption capacity, activated carbons with very high surface area and porosity are promising candidates for storage applications and in separations involving high pressures (such as pre-combustion capture and natural gas sweetening) [18–22]. Moreover, they could constitute a starting point for the development of chemically modified and more complex composite materials [21,23–25] with enhanced affinity and selectivity for carbon dioxide. These considerations provide a motivation to explore properties of high surface area activated carbons

* Corresponding author.
E-mail address: Lev.Sarkisov@ed.ac.uk (L. Sarkisov).

http://dx.doi.org/10.1016/j.carbon.2015.06.056
0008-6223/

in application to carbon capture in more detail with a particular focus on multi-component mixtures, including water.

Previous experimental studies on carbonaceous materials and carbon dioxide adsorption from mixtures mainly involve binary (CO_2/CH_4) and ternary ($CO_2/CH_4/N_2$) systems in the absence of water vapor, see for example Refs. [20,26–29]. Wu et al. also reported experimental measurements and predictions for the quaternary mixture $H_2/N_2/CH_4/CO_2$ [30].

Studies based on single component isotherms have also been used to predict the behavior of the mixtures; for example, Herm et al. [31] applied the Ideal Adsorbed Solution Theory (IAST) [32] to the data published in the comprehensive work by Sircar et al. [14] to predict the behavior of CO_2/H_2 mixtures in BPL activated carbon in comparison with the behavior of several metal–organic frameworks. In another example, Himeno et al. considered adsorption of methane and carbon dioxide on several carbon materials and also employed IAST to predict behavior of binary mixtures [20].

Simulation studies include the works by Cracknell et al. [33] on CO_2/N_2 and CO_2/CH_4 mixtures, by Heuchel et al. [34] on CO_2/CH_4 mixtures, by Sweatman and Quirke on ternary $CO_2/CH_4/CO$ mixtures [35] and the work by Cao and Wu [36] on CO_2/H_2 mixtures. In all these studies the slit pore model was used to represent the carbon structure. More recent simulation studies considered CO_2/CH_4 mixtures using more realistic models of activated carbons [37–39]. In particular, Furmaniak and co-workers systematically explored how the efficiency of the separation of CO_2/CH_4 mixtures depends on the surface oxidation and on the pore size in virtual porous carbons (VPC) [38]. Further examples of binary mixtures in disordered models (although not necessarily related to CO_2 capture) include the studies by Kumar and co-workers [40,41].

All multi-component streams involved in the CO_2 capture processes are prone to contain water in various amounts, depending on the process, and therefore it is important to include water into consideration. Adsorption of water on activated carbons has been a long standing problem. An important and comprehensive review on the experimental and computational studies in the field has been published by Brennan et al. [42]. In particular, the authors summarized substantial developments in our understanding of the role of polar surface groups on water adsorption in activated carbons, arising from a number of studies in the area [43–46], to which there have also been more recent important experimental and simulation contributions [47–53]. Brennan and co-workers [54] investigated the problem in a study, where the structure of an activated carbon was represented through a realistic, disordered model, obtained from the Reverse Monte Carlo simulation and featuring variable number of functional groups. Liu and Monson [55], Horikawa et al. [56] and Wang et al. [57] also studied the effect of structural and surface chemical heterogeneities on water adsorption and desorption in activated carbons. In particular, Liu and Monson simulated adsorption of water on a model consisting of a random packing of platelet shaped elements featuring functional groups, developed from the model first proposed by Segarra and Glandt [58]. Do and co-workers developed a series of models to understand the mechanism of water adsorption in micro- and mesopores of activated carbons, based on the growth of a water cluster around a functional surface group [56,59–61]. These models have been subject of further modifications and studies [56,62–65].

To summarize substantial number of observations, accumulated from both computer simulations and experiments, water shows a very peculiar behavior when adsorbed on activated carbon. The surface of activated carbons is in general hydrophobic, but it does contain heteroatoms (most commonly oxygen, nitrogen and sulfur), often in the form of polar groups. It is precisely in the proximity of these hydrophilic centers where the adsorption of water is believed to start. The first molecules adsorbed around the hydrophilic centers through hydrogen bonding then function as nuclei around which water clusters can grow. It has been shown that the higher the concentration of functional groups in carbon is, the higher the extent of water adsorption at low pressure is, while an increase in the number of functional groups can lead to a substantial change in the shape of the isotherm [42]. Given enormous interest in water adsorption on activated carbons, the number of studies on the impact of humidity on adsorption of other species is surprisingly modest. The effect of water presence on carbon dioxide adsorption from mixtures and under conditions resembling real industrial cases has been investigated to an even lesser extent.

The majority of the work which has been published so far is experimental. Several studies in this context explore adsorption of carbon dioxide, methane and other gases on humid activated carbon or coal. For example, comparative pure component adsorption of methane and carbon dioxide on coal in the presence of water was investigated by Krooss et al. [66]. A similar study on activated carbons has been carried out by Wang et al. [67]. Sun et al. assessed the effect of humidity on the pure component adsorption of CO_2 on activated carbon [68]. In another study, Sun and co-workers also investigated adsorption of CO_2/CH_4 mixture on activated carbon in the presence of water [69]. Billemont and co-workers employed both experiments and grand canonical Monte Carlo simulations to explore single component and binary mixture adsorption for carbon dioxide and methane on humid porous carbons [70,71]. As a model of the carbon structure they considered both the classical slit pore model and a more realistic disordered structure. In the case of the disordered structure they studied two systems, one featuring and one not featuring any functional groups.

Other experimental studies include the work by Fitzgerald et al. on the ternary mixture of carbon dioxide, methane and nitrogen, adsorbing on humid Tiffany coal [72]. Finally, Xu and co-workers investigated the realistic case of the effect of water on CO_2 capture from the model flue gas using vacuum swing adsorption (VSA) process on activated carbon [73,74]. Their study involved quaternary $N_2/CO_2/O_2/H_2O$ mixture.

What in general emerges from all these studies is the fact that *small* amounts of humidity in the mixtures do not change the shape of the adsorption isotherms and do not influence the pore filling mechanism, but they do have an effect in decreasing the adsorption, to an extent proportional to the amount of water present in the system. The decrease in the adsorption may actually be hardly noticeable, if the amount of water is very small. It has also been shown that species forming hydrates under conditions of interest may be preferentially adsorbed [69].

Overall, although a substantial body of work on multicomponent adsorption in activated carbons has been accumulated, not many studies so far have considered conditions representing operational temperatures, pressures or compositions of the streams associated specifically with the CO_2 capture processes. In the majority of the cases the studies involved pure component isotherms or equimolar binary mixtures at 298 K, and the presence of minor components has rarely been considered. The effect of small amounts of water on adsorption of other species specifically in the context of capture processes also needs to be addressed. Finally, we are not aware of any systematic studies of these issues in application to high surface area (>3000 m^2/g) activated carbons, although they seem to be a promising class of materials for some of the carbon capture related processes. This provides the motivation for this work.

In our previous publication [75] we developed a realistic molecular model for Maxsorb MSC-30, an activated carbon which has been commercially produced by the Kansai Coke and Chemicals

since 1990s and shows surface area in excess of 3000 m^2/g [18,76]. The model is based on representing the structure of Maxsorb as a random packing of corannulene-like molecules, functionalized with hydroxylic groups and is similar to other models developed in this spirit [38–40,77]. While capturing the disordered nature of the activated carbons these models remain somewhat more computationally tractable than more realistic models based on the reconstruction of the structure through Reverse Monte Carlo [78–80]. Chemical composition of our previous model, including the amount of oxygen present, and its structural characteristics, such as surface area and pore volume, have been tuned to closely reflect these parameters for Maxsorb. The developed model was calibrated and tested through the comparison to the experimental single component isotherms for carbon dioxide and some of the main components of the streams involved in carbon capture processes.

In this study we apply this model to explore Maxsorb behavior with respect to multi-component mixtures, representative of different carbon capture processes under realistic conditions, including presence of water vapor in the streams. We begin by the analysis of single component water adsorption followed by binary mixtures, consisting predominantly of carbon dioxide with small amounts of water present. Finally, we investigate more complex, multi-component systems in the context of pre- and post-combustion capture and natural gas sweetening. We emphasize here that the current contribution does not consider kinetics and transport aspects of adsorption processes, although they are important in the complete design analysis; this will be subject of a separate study.

2. Methodology

2.1. Molecular model of Maxsorb, MSC-30

The molecular model of Maxsorb MSC-30 has been developed in our previous study [75] and is based on a random packing of corannulene-like (therefore curved) structural elements, functionalized with hydroxyl groups.

Fig. 1 shows two views of the structural element ((a) and (b)) and the final structure obtained after random packing (c). The structure contains 250 elements in a cubic cell with a side length of 60 Å. The model was developed to reproduce key structural characteristics of MSC-30 (but we note that the current approach is not concerned with the mechanical stability of the model structures) and comparison between the properties of the model (from now on named CRNL-$(OH)_2$) and the prototype material is provided in Table 1 [75]. From Table 1 it is possible to see that the features of the model quite closely follow the features of the target material. However, unlike the actual Maxsorb material featuring pores mostly around 20 Å and up to 60 Å in diameter [18], the current model is microporous with pores not exceeding 10 Å (the geometrical pore size distribution and associated discussion are provided in the Supplemental Information (SI) file, Section 10).

Table 1
Characteristics of the model structure based on a packing of corannulene-like elements functionalized with two hydroxyl groups (CRNL-$(OH)_2$), compared to the experimentally measured typical properties of Maxsorb MSC-30 (MSC-30) [75]. In this table, S.A. is the surface area, V is the micropore volume, K_H is the Henry's constant of adsorption and C/O is the carbon/oxygen ratio (in weight) in the material.

System	S.A. (m^2/g)	V, 298 K (cm^3/g)	K_H CH_4, 298 K (mol/kg/Bar)	K_H CO_2, 298 K (mol/kg/Bar)	C/O
CRNL-$(OH)_2$	3236.64	1.28	1.03	1.96	7.5
MSC-30	3000–3400	1.3–1.7	1.3–1.9	2.4	7.8

Surface area and micropore volume (from computational Helium porosimetry) of the packing of structural elements have been calculated using Poreblazer 1.2, a package of simulation tools developed by Sarkisov and Harrison [81]. The Henry's constants of adsorption in zero loading regime have been calculated using a simple approach, recently proposed by Sarkisov [82], based on the lattice representation of the simulation cell. Further details on the construction and characterization of the model can be found in our previous publication [75].

2.2. Simulation details

For all our simulations we use the energy biased grand canonical Monte Carlo method (GCMC), as implemented in the MuSiC simulation package [83]. Further details of the GCMC simulation protocol adopted in this work, including details of the potential cut-offs, number of Monte Carlo moves per adsorption point, type and weight of Monte Carlo moves and other parameters, are provided in the Supplemental Information (SI, Section 1) file.

For consistency with the experimental measurements and following the procedure proposed by Talu and Myers [84], unless specified otherwise, all the simulated adsorption densities are converted into excess values using the following expression:

$$N_{exc} = N_{abs} - V \cdot \rho_{bulk} \quad (1)$$

where N_{exc} is the excess adsorption, N_{abs} is the absolute adsorption as calculated from the GCMC simulation, ρ_{bulk} is the density of the bulk adsorbate and V is the accessible pore volume, as obtained from the computational Helium porosimetry. To calculate the bulk density we perform a separate, GCMC simulation of the bulk phase. This aims to minimize the error intrinsically associated with the

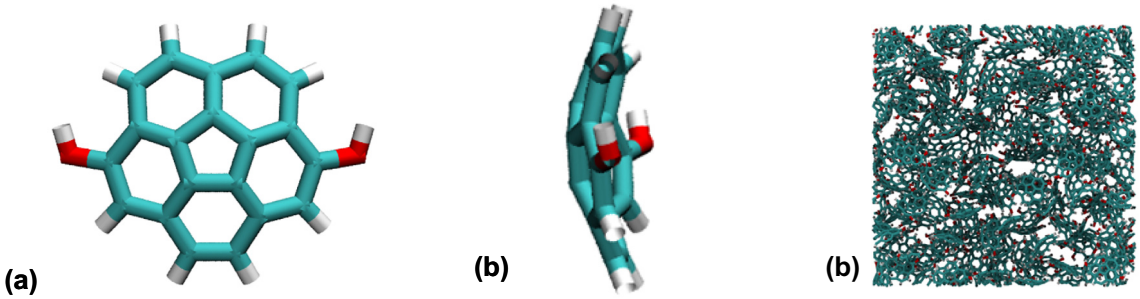

Fig. 1. Computer visualizations of a corannulene-like element functionalized with two hydroxylic groups from two different perspectives (panels (a) and (b)) [75]). The final structure (250 elements in a cubic cell of 60 Å in size) obtained from random packing of the individual elements is shown in panel (c). Cyan: carbon, red: oxygen, white: hydrogen. (A color version of this figure can be viewed online.)

differences in fluid properties predicted from the forcefield models and from the equation of state (EOS) methods. This is particularly important for high pressure multi-component mixtures, where these differences may become significant.

The full set of Lennard-Jones (LJ) parameters associated with the model structure for the adsorbent is reported in the SI (Section 2). The LJ parameters mostly correspond to the ones proposed by Tenney and Lastoskie [85], which are also in line with other parameters reported in literature [86–90]. Partial charges are calculated using the B3LYP Density Functional Theory method [91], with 6-31G basis set and CHELPG [92] charge analysis using the Gaussian 09 software package [93].

For the adsorbates involved in the simulations, TraPPE models [94–97] are used where available; hydrogen is represented using the spherical model by Buch [98] and carbon monoxide is modeled using the two-center model with partial charges by Sweatman and Quirke [99]. For water the tip4p model is adopted, which exhibits a reasonable accuracy in capturing VLE properties of water at ambient conditions [100]. It would be of a further interest to investigate other models of water.

A table with the bond lengths and bond angles for the molecular species (except for hydrogen and methane, modeled as single Lennard-Jones sites) and a table with the full set of partial charges and Lennard-Jones parameters are reported in the SI (Section 2). We note here that all the adsorbing species are treated as rigid molecules.

The LJ solid–fluid interactions are calculated using the standard Lorentz–Berthelot mixing rules, but a scaling factor of 1.23 is applied to the platelet carbon – fluid LJ interaction for species with molecular models featuring no explicit charges, such as methane and hydrogen, following the calibration performed in the previous publication [75]. All solid–fluid interactions are pre-calculated using a cubic lattice with 0.2 Å resolution prior to the adsorption simulations.

Fluid–fluid Coulombic interactions between partial charges are calculated using the Fennell–Gezelter method [101] based on a spherically truncated summation, while in the solid–fluid case the Ewald summation [102] is applied. In the SI file we also provide a comparison between the Fennell–Gezelter and Ewald methods for fluid–fluid interactions, considering a case of confined water (Section 3).

In all cases considered we show some exemplary adsorption isotherms, accompanied by the analysis of selectivities for the main separations, defined as:

$$S_{i/j} = \frac{x_i/x_j}{y_i/y_j} \tag{2}$$

where $S_{i|j}$ is the selectivity for component i over component j; x_i, x_j are the molar fractions of components i and j in the adsorbed phase (calculated form the absolute adsorption); y_i, y_j are the molar fractions of components i and j in the bulk phase.

For the same mixtures we also predict selectivities in the Henry's law regime using the formula:

$$S^H_{i/j} = \frac{K_{H,i}}{K_{H,j}} \tag{3}$$

where $S^H_{i/j}$ is the selectivity for component i over component j in the Henry's law region, while $K_{H,i}$ and $K_{H,j}$ are the Henry's constants for components i and j, respectively.

Selectivity can give a good indication on how efficient the separation of the components in a mixture can be, but nevertheless it is not the only criterion that needs to be taken into account for the assessment of carbon capture materials: for example, high values of selectivity do not necessarily imply high efficiency in a certain separation, since they may also correspond to very high affinity toward one of the components in the mixture and therefore high costs associated with adsorbent regeneration. Hence, a complete analysis must be based on selectivity in conjunction with other characteristics such as high working capacity, affordable cost of material, stability to water and so on. In general, the most comprehensive assessment of a material should come from a process simulation [103,104].

3. Results

This section consists of two parts. In the first part we focus on adsorption of water in a platelet-based model of Maxsorb activated carbon. Specifically, we start with a single component case and explore the role of surface groups in the formation and growth of water clusters. We then consider co-adsorption of carbon dioxide and water with a view to understand the possible influence of water on carbon capture process. In the second part of the Results section we consider equilibrium adsorption of multicomponent mixtures with the composition and under conditions, corresponding to the specific industrial carbon capture processes.

3.1. Water adsorption in Maxsorb MSC-30

3.1.1. Single component case

Fig. 2 compares adsorption isotherm for water from molecular simulations at 298 K (absolute density, black squares for adsorption and red squares for desorption) to two sets of the experimental data at 303 K (from Carlile and Friday [105], gray squares, and Miyawaki and co-workers [47] (white squares), with the SAC31 material in their work corresponding to a sample of Maxsorb material[1]. The simulated isotherm exhibits a convex shape, typical for water adsorbing in hydrophobic materials, followed by a capillary condensation at $p/p^\circ = 1.0$. We note that the simulated isotherm is shifted to higher pressures compared to the experimental results and reaches density plateau at pressures exceeding the bulk condensation pressure (which for tip4p model of water is 4.5 kPa at 298 K [106]; this is also the reason for presenting simulation results in the absolute adsorbed density units. However the difference between the excess and absolute amount adsorbed is expected to be insignificant at pressures below the bulk condensation pressure). It also features a broad hysteresis loop and appears in shape as Type V isotherm, according to the IUPAC classification [107]. A detailed isotherm by Miyawaki and co-workers [47] also exhibits smooth *S*-shape behavior, with no evident jumps in density, unlike the isotherm from molecular simulations. Experimental results by Miyawaki et al. also point to a higher adsorption capacity of about 75 mmol/g, compared to the results from molecular simulations (about 60 mmol/g at the highest loading). It is also important to note substantial differences between the two sets of the experimental data, suggesting that consistent measurement of water adsorption on activated carbons still presents a substantial challenge.

It has been widely accepted that the surface groups play an important role in the water uptake process. To illustrate this, we contrast the behavior of the original model for Maxsorb with that of the model featuring no surface groups. To make this comparison consistent and isolate the effect of the surface groups from other factors we consider a system, based on non-functionalized coranulene elements, with structural characteristics (such as surface area, pore volume and density) very similar to the original model of Maxsorb MSC-30. Structural characteristics of the two models are compared in Table 2.

In Fig. 3 we show absolute water adsorption isotherms simulated at 298 K for the original CRNL-$(OH)_2$ model (black symbols),

[1] K. Kaneko, Personal communication.

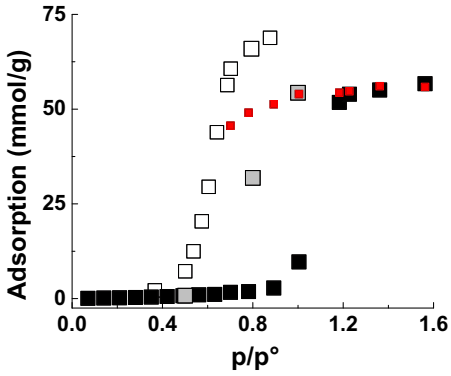

Fig. 2. Water adsorption isotherms on Maxsorb MSC-30. Black and red squares: simulation results at 298 K for adsorption and desorption, respectively; gray squares: data by Carlile and Friday at 303 K [105], white squares: data by Miyawaki et al. at 303 K [47]. (A color version of this figure can be viewed online.)

Table 2
Characteristics of the model structures based on corannulene-like elements functionalized with hydroxyl groups (CRNL-$(OH)_2$), and on non-functionalized corannulene-like elements (CRNL). In this table, S.A. is the surface area, V is the micropore volume and ρ is the density.

System	S.A. (m^2/g)	V, 298 K (cm^3/g)	ρ (g/cm^3)
CRNL-$(OH)_2$	3236.64	1.28	0.54
CRNL	3241.72	1.30	0.52

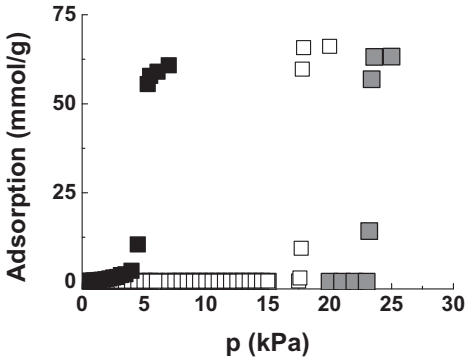

Fig. 3. Absolute adsorption isotherms for water at 298 K from molecular simulations. Black symbols correspond to the original Maxsorb MSC-30 model (CRNL-$(OH)_2$). White symbols are for the system with no functional groups. The system still features partial charges associated with the carbon atoms of the platelets and termini hydrogens. Gray symbols correspond to the system with no functional groups and no Coulombic interactions between the platelets and water molecules.

compared to the isotherms simulated on the model without functional groups (CRNL with the properties reported in Table 2). White and gray symbols correspond to two slightly different variants of the second model: in the case of white symbols the model still features partial charges on the edges of the platelets associated with the termini hydrogen atoms, while in the case of the gray symbols no solid–fluid Coulombic interactions are taken into account.

It is clear that the presence of the functional groups substantially changes the adsorption behavior of water. The isotherms in the models featuring no functional groups are shifted to much higher pressures, and this is in agreement with the results by Billemont and co-authors [71], which show that the presence of oxygenated groups in a sparse model for activated carbon determines an increase in the amount of adsorbed water at a given pressure. Similar results were also shown in the work by Brennan and co-workers [54], in which the adsorption of water was found to be proportional to the amount of functional groups on the structure of the carbon.

Let us consider in more detail processes on molecular level associated with the formation and growth of the water clusters in the model structure. First, we need to define a cluster. Two water molecules are considered to be connected if the distance between their oxygen atoms is less than 3.5 Å (this distance corresponds to the first minimum in oxygen–oxygen radial distribution function for the bulk liquid water at ambient conditions). A pathway, consisting of these pairwise connections can be constructed for any two water molecules within a cluster. In the system with functional groups, formation of a cluster starts with association of a water molecule with one of the groups. In Fig. 4 we show a system involving one platelet and one molecule of water in the lowest potential energy configuration, whereas Table 3 summarizes contributions of Lennard-Jones and Coulombic terms to the total potential energy in this configuration. As can be seen from the figure the water molecule forms a hydrogen bond with the surface group. This association is predominantly governed by the Coulombic interaction (Table 3).

In Fig. 5 we show the water clusters respectively for the system with groups (top panel) and the system without groups but still bearing charges on carbon atoms and termini hydrogens (bottom panel). In all cases what is actually shown are the oxygen atoms in each cluster, with different colors corresponding to different clusters.

Table 3
Contributions to the total solid–fluid interaction energy for a system of a single platelet and a water molecule in the minimum potential energy configuration. Energies are expressed in kJ/mol.

Lennard-Jones	4.39
Coulombic	−29.42
Total	−25.03

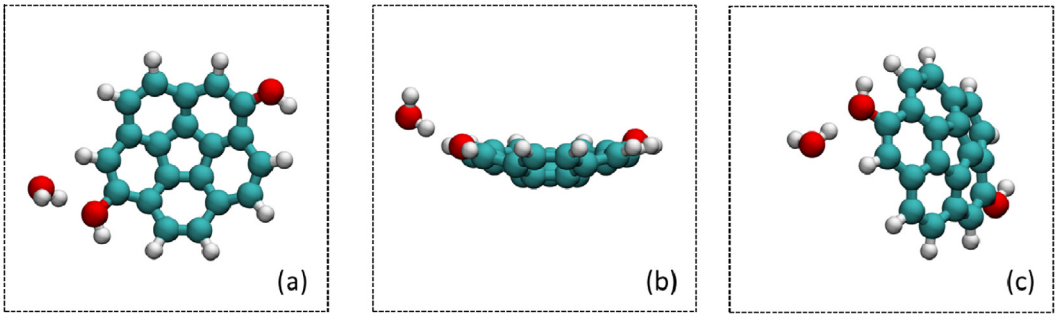

Fig. 4. Computer visualization of the minimum potential energy configuration of a single water molecule and one platelet. The snapshots correspond to different view angles of the same configuration. Cyan: carbon, red: oxygen, white: hydrogen. (A color version of this figure can be viewed online.)

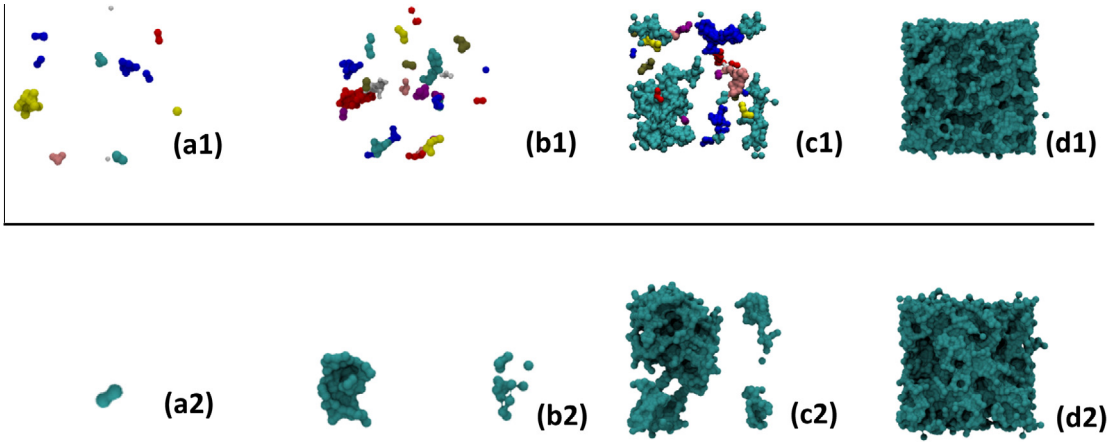

Fig. 5. Visualizations of oxygen atoms in water clusters formed during simulation on the model featuring functional groups (top panel) and the model featuring no functional groups (bottom panel) at different pressures. In the top panel (a1): 2.20 kPa, (b1): 3.5 kPa, (c1): 4.5 kPa, (d1): 7 kPa; different colors correspond to different clusters. In the bottom panel (a2): 17.5 kPa, (b2): 17.6 kPa, (c2): 17.7 kPa, (d2): 17.8 kPa; at all pressures only one cluster is present, shown in periodic boundary conditions. (A color version of this figure can be viewed online.)

The behavior is very different in two cases. In the model of Maxsorb, featuring functional groups, condensation starts at low pressure (the lowest pressure shown in Fig. 5(a) is 2.2 kPa, however the clusters actually start to appear at as low as 0.63 kPa). Several small clusters form around functional groups, and as the simulation progresses these clusters grow in size, until one percolated cluster spanning the whole system forms.

In the case of the material with no functional groups the onset of cluster formation is delayed to much higher pressures (17.5 kPa), and the following process corresponds to gradual growth of one cluster, as opposed to many clusters developing in parallel as in the first case. The process, as described by the snapshots in the bottom panel of Fig. 5, occurs within a very narrow pressure range between 17.5 kPa and 17.8 kPa.

To summarize, the current model overestimates the hydrophobicity of the Maxsorb MSC-30 structure, resulting in the adsorption isotherm shifted to higher pressures and exhibiting an abrupt capillary transition, not observed in experiments. Behavior of water is very sensitive to the concentration of the functional groups and most likely to their nature. We speculate that introduction of a higher number of functional groups, other, more polar or more accessible functional groups in the model should shift the water adsorption isotherm to lower pressures and induce larger number of intermediate adsorption states, corresponding to more water clusters simultaneously growing in the system. Given that the current results are obtained with 300–900 million Monte Carlo moves per adsorption point, this systematic exploration of water behavior as a function of model features is however a computationally challenging task and will be considered as a separate study.

3.1.2. Effect of water on carbon dioxide adsorption in Maxsorb MSC-30

Before we turn our attention to more complex, multi-component systems, first, it is important to explore in more detail co-adsorption of carbon dioxide and water under different conditions. It is instructive to begin this section by comparing the Henry's constants of adsorption in zero loading regime for pure component carbon dioxide and water at three different temperatures (298, 313 and 323 K). These constants, summarized in Table 4, indicate much stronger interaction of water molecules with the porous structure (or to be more precise with the functional groups), which can explain stronger adsorption of water compared to other gases as will be seen in the next section.

Nevertheless, from the appearance of the water isotherms, Maxsorb behaves as a typical hydrophobic material. This is a result of even stronger interaction between molecules of water itself, compared to the interaction with the porous material, particularly once the polar groups on the structure of the carbon, already saturated with water molecules, become unavailable.

Table 4
Henry's constants of adsorption calculated for water and carbon dioxide at three different temperatures.

T (K)	K_H (mol/kg/Bar)	
	CO_2	H_2O
298	1.96	23.49
313	1.34	10.68
323	1.07	6.72

The zero loading (this is the regime reflecting the most favorable interactions) isosteric heat of adsorption is estimated to be 40.13 kJ/mol, which is comparable to the latent heat of condensation for water (45 kJ/mol). This result is in line with the data reported in literature [43,108].

The mechanism of carbon dioxide interaction with a single platelet is different from that of water. In Fig. 6 we show the configurations corresponding to the energy minima of system of a single carbon dioxide molecule and a platelet. Panels on the left visualize the global energy minimum, with the carbon dioxide molecule positioned not on the edge but above the center of the platelet. Panels on the right show an example of a local energy minimum configuration for carbon dioxide molecule in the vicinity of a hydroxyl group. Comparison of the energy contributions for the two cases, provided in Table 5, shows that the global energy minimum is dominated by the Lennard-Jones contribution, emanating from the carbon atoms of the platelet. In the vicinity of the surface group, Coulombic term increases substantially (about seven times), but this is not enough to compensate for the weaker LJ interactions at the edge of the platelet. The global energy minimum for carbon dioxide is significantly shallower (in a sense that the interaction is weaker) compared to the water molecule.

Next, we investigate the effect of small amounts of water present in the stream on carbon dioxide adsorption under typical pre-combustion conditions. In this case the total pressure of the streams ranges between 30 and 55 Bar at 313 K and the water content ranges between 0.2 and 1% (molar) [6]. Several binary mixtures of water and carbon dioxide are investigated at a typical temperature of 313 K with different amounts of water present. For these mixtures, adsorption isotherms are extended up to the

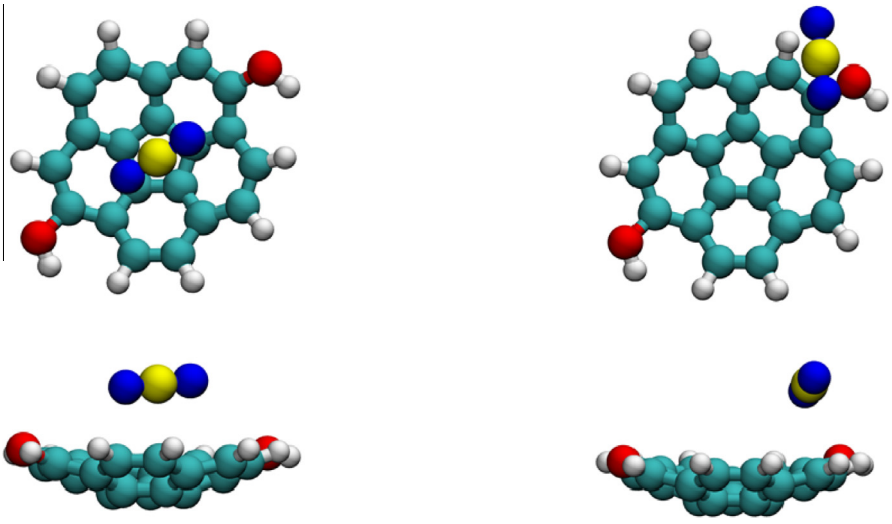

Fig. 6. Minimum potential energy configurations for a single carbon dioxide molecule in the presence of a single platelet. Panels on the left show two alternative views of the global energy minimum configuration, panels on the right show a local energy minimum in the vicinity of the surface group, also from two alternative perspectives. For the platelet the color scheme uses cyan for carbon, red for oxygen, white for hydrogen. For the carbon dioxide molecule, yellow is used for carbon and blue for oxygen, for greater contrast. The atom particles are not to scale. (A color version of this figure can be viewed online.)

Table 5
Solid–fluid interaction energies calculated for preferential positions of carbon dioxide molecules in the proximity of one platelet. The cases of global and local energy minima (corresponding to the configurations in Fig. 6) are shown on the left and right, respectively. Energies are expressed in kJ/mol.

Energy minimum	Global	Local
Lennard-Jones	−15.03	−4.60
Coulombic	−0.92	−7.21
Total	−15.95	−11.81

dew point where the partial pressure of water reaches the saturation value, 7.33 kPa at 313 K. Dew points for various water amounts in the mixture are summarized in the SI file (Section 9).

From Fig. 7(a), water does not seem to have any impact on the adsorption of carbon dioxide in the range of pressures under consideration. The isotherms in graph (b) confirm the results shown in graph (a) and the amount of water adsorbed remains small under conditions of interest. This is predominantly due to the overwhelming excess of carbon dioxide in the binary mixture.

In Section 3.1.1 we have investigated the tendency of water to cluster during the single component adsorption on Maxsorb, and we have shown that clusters start to appear from relatively low pressures. According to the analysis of the minimum energy configurations, carbon dioxide and water should occupy different, non-overlapping regions of the porous space, at least at lower pressures. To probe this picture further we set to investigate a series of systems with substantially larger amount of water present. Specifically, we prepared systems featuring 2:1 ratio of carbon dioxide to water (mole basis) and total loading of 24 mmol/g, 1:1 ratio and total loading of 30 mmol/g and 1:2 ratio and total loading of 36 mmol/g, respectively, and investigated structural characteristics of these systems at 313 K under NVT conditions.

In Fig. 8 we show the radial distribution functions (RDFs) for water (graph (a)) and carbon dioxide (graph (b)) for different pressure points on the isotherms simulated at 313 K. In the case of water we show the O–O RDF, while for carbon dioxide we show the C–C RDF.

In the case of H_2O the peaks in the RDFs appear similar in shape to those reported for bulk water (including the tip4p model) at elevated temperatures [109,110]. The pronounced first peak can be seen simply as a manifestation of strong water–water interactions. We also note that even at the lowest water concentration (green line), the RDF for water starts to develop a second peak, indicating onset of more of a liquid-like structure. Carbon dioxide exhibits RDFs typical for a gaseous substance and consistent with the results reported in the literature for supercritical CO_2, [111,112].

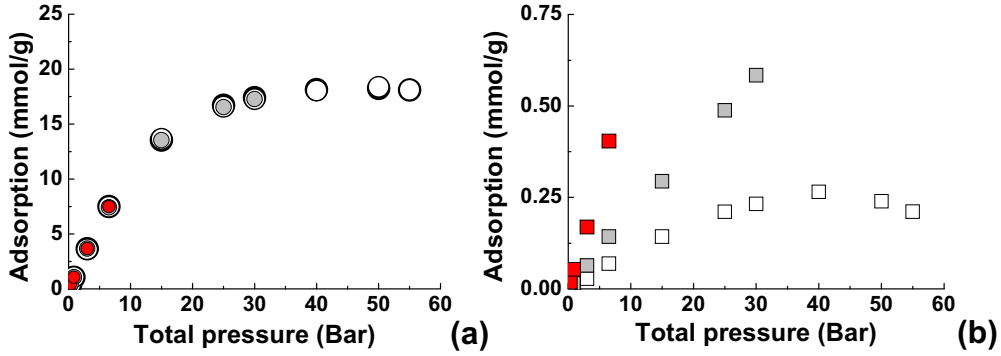

Fig. 7. Excess adsorption isotherms for CO_2 (on the left, panel (a)) and H_2O (on the right, panel (b)) at 313 K corresponding to binary CO_2/H_2O mixtures with different water content. Black symbols are for 0% (panel (a) only), white symbols are for 0.1% (mole), gray symbols are for 0.2% and red symbols are for 0.5% water. (A color version of this figure can be viewed online.)

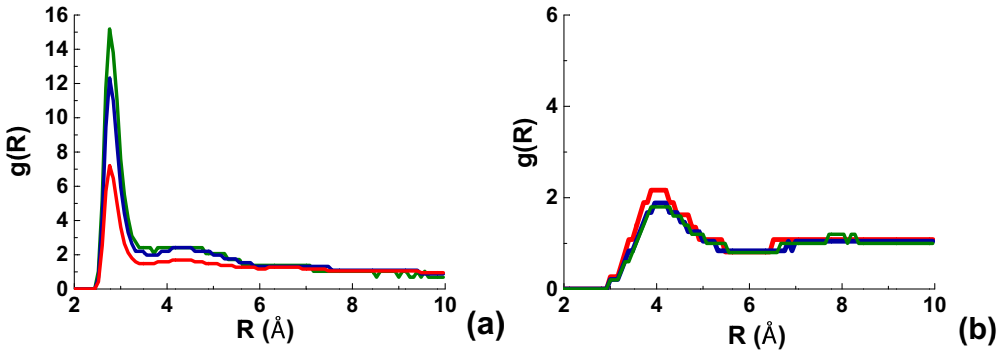

Fig. 8. (a) Radial distribution function for water (O–O RDF); (b) radial distribution function for carbon dioxide (C–C RDF) at 313 K. Green lines correspond to CO_2/H_2O = 2:1 and total loading of 24 mmol/g; blue lines correspond to CO_2/H_2O = 1:1 and total loading of 30 mmol/g and red lines correspond to CO_2/H_2O = 1:2 and total loading of 36 mmol/g, respectively. (A color version of this figure can be viewed online.)

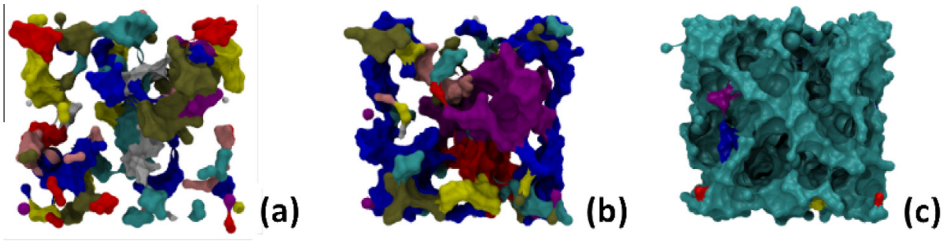

Fig. 9. Visualizations for water clusters in the mixtures carbon dioxide and water simulated at 313 K; (a) CO_2/H_2O = 2:1 and total loading of 24 mmol/g; (b) CO_2/H_2O = 1:1 and total loading of 30 mmol/g; (c) CO_2/H_2O = 1:2 and total loading of 36 mmol/g. Colors correspond to different clusters, based on the positions of oxygen atoms of water molecules. (A color version of this figure can be viewed online.)

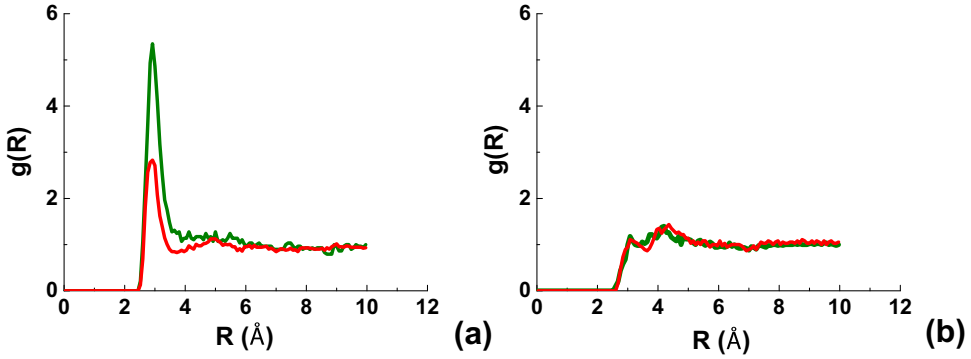

Fig. 10. Solid–fluid radial distribution functions for adsorbed water (graph (a)) and carbon dioxide (graph (b)) in the binary CO_2/H_2O system at 313 K. The functions are calculated considering oxygen atom for water, carbon atom for carbon dioxide and oxygen atom belonging to the hydroxylic functional group for the adsorbent. Green lines are for CO_2/H_2O = 2:1 composition and total loading of 24 mmol/g; red lines are for CO_2/H_2O = 1:2 composition and total loading of 36 mmol/g. (A color version of this figure can be viewed online.)

The visualizations for the water clusters in the three mixtures are reported in Fig. 9. Similar to the single component case, water adsorption can be seen as formation and growth of different clusters, which eventually merge into a single one at higher concentrations of water (as long as the porous space itself is percolated with respect to water molecules).

Finally, we calculate solid–fluid radial distribution functions for the same CO_2/H_2O mixtures considered above, both for water and carbon dioxide. For the adsorbate species, the RDFs are calculated considering the same atoms as for the fluid–fluid RDFs before, while for the adsorbent we use the oxygen atom belonging to the hydroxyl group. The results are presented in Fig. 10, which shows the solid-water RDF in graph (a) and the solid-carbon dioxide RDF in graph (b). In both cases systems corresponding to CO_2/H_2O = 2:1 and total loading of 24 mmol/g (green lines) and CO_2/H_2O = 1:2 and total loading of 36 mmol/g (red lines) are considered.

From Fig. 10 we can clearly see pronounced peaks for the solid-water RDFs at distances below 3.5 Å (left side panel), with the second peak developing at the higher loading; RDFs for carbon dioxide do not feature any pronounced peaks, indicating essentially no density variations around hydroxyl groups of platelets. The composition does not seem to have an important effect for the carbon dioxide structure.

The results shown so far suggest that at low and moderate pressures water and carbon dioxide preferentially occupy different sub-regions in the porous space; indeed, water molecules prefer proximity of heteroatoms or, more in general, of polar centers, whereas carbon dioxide prefers the curved surface of the platelet, as shown by the energy minimization analysis. Therefore, under

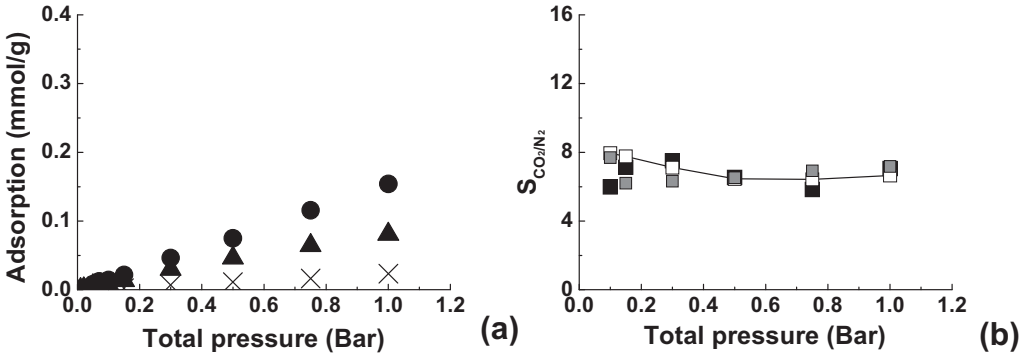

Fig. 11. (a) Excess adsorption isotherms for the mixture $CO_2/N_2/O_2$ = 15/80/5. Circles are for CO_2, triangles are for N_2, crosses are for O_2. (b) Carbon dioxide/nitrogen selectivities as a function of pressure for binary mixture CO_2/N_2 = 50/50 (black squares), binary mixture CO_2/N_2 = 10/90 (white squares and a black line) and ternary mixture $CO_2/N_2/O_2$ = 15/80/5 (gray squares). The line is for eye guidance only.

conditions of interest two species may co-adsorb without much influence on each other. This analysis applies to fragments functionalized with hydroxyl groups. We speculate it should remain valid for other groups containing oxygen, such as carboxylic and lactonic surface groups. However, nitrogen containing groups, such as amines, should be further investigated.

3.2. Simulation of carbon capture separation processes

3.2.1. Post-combustion carbon capture from flue gas

Flue gas is predominantly comprised of nitrogen, with carbon dioxide constituting about 15% of the mixture at the total pressure of about 1 Bar and temperatures between 50 and 100 °C [6]. Flue gas also contains a certain amount of water vapor (5–7%) and small amounts of oxygen, nitrogen oxides (NO_x) and sulfur oxides (SO_x). The main separation we investigate in this case is between N_2 and CO_2. After consideration of the equimolar mixture case we shift to a mixture of molar composition CO_2/N_2 = 10/90, more closely reflecting industrially relevant conditions, and then we will progressively add other, minor components to the system, to study ternary mixtures of CO_2, N_2 and O_2 (15/80/5) and quaternary mixtures of CO_2, N_2, O_2 and H_2O (15/75/5/5) with molar percentages of the components given in the brackets. All simulations are at 323 K, as this temperature can be considered representative for the post-combustion processes. To make presentation more compact, we predominantly focus on CO_2/N_2 selectivity in various systems, while the actual isotherms are shown for illustration purposes for several selected cases only.

An example of excess adsorption isotherms for a ternary mixture is shown on the left of Fig. 11, while on the right we summarize selectivity behavior for binary and ternary systems as a function of pressure. The lowest value of pressure considered in Fig. 11(b) is 0.1 Bar, as pressures around 0.1–0.15 Bar have been recognized as a reasonable lower limit for the desorption processes involving flue gas separations [8].

In general, all systems in the figure exhibit selectivity values between 6 and 8. In particular, we notice that for the binary mixtures (black and white squares) a change in the molar composition has almost no effect on the selectivity. Addition of oxygen to the mixture also seems to have minor effect on the overall CO_2/N_2 selectivity. Finally, zero loading, intrinsic CO_2/N_2 selectivity, is calculated to be 6.59 at 323 K.

The observed selectivity values are typical for activated carbons. For example, selectivity of activated carbon AX21 with respect to the equimolar mixture at 293.1 K up to 1 Bar ranges approximately between 6 and 7, as calculated by Kluson and Scaife [113] by applying IAST to the single component experimental isotherms. We further note that these values of CO_2/N_2 selectivity are rather low compared to other materials such as zeolites [114–116] and metal–organic frameworks, which routinely exhibit selectivity above 20 [6,7,117–119].

From Fig. 11, the values of selectivity remain relatively independent of pressure; some variation at low pressure is expected as the number of nitrogen molecules adsorbed is small and selectivity becomes subject of large fluctuations and statistical error. For example, at the total pressure of 0.1 Bar for the CO_2/N_2 equimolar mixture the error in selectivity reaches 44.6%, while at 1 Bar the error is approximately 12.8%.

Fig. 12 shows the effect of a relatively small amount of water (5%) on co-adsorption of carbon dioxide, nitrogen and oxygen. Water saturation pressure at 323 K is 12.26 kPa and the total pressure of the mixture, at which water should start to condense (2.45 Bar) is outside of the pressure range considered here. In panel (a) on the left of Fig. 12 we report the excess adsorption isotherms for the mixture with the composition $CO_2/N_2/O_2/H_2O$ = 15/75/5/5, while in panel (b) on the right the CO_2/N_2 selectivities are shown as a function of pressure for the same mixture (red symbols and lines) in addition to the selectivities previously shown in Fig. 11(b).

From comparison of Figs. 11 and 12, the effect of water on the CO_2/N_2 separation appears negligible. At the same time it is clear that the amount of adsorbed water substantially exceeds all the other adsorbed species, so that water is the preferentially adsorbed species.

Overall, in terms of CO_2/N_2 selectivity Maxsorb does not come across as the best candidate for CO_2 capture from flue gas, especially because key advantages of this material, such as high adsorption capacity at high pressures, cannot be exploited in this context.

3.2.2. Pre-combustion carbon capture

A preliminary analysis of water impact on carbon dioxide adsorption has been given in Section 3.1.2. Here we extend it to multicomponent mixtures. In the pre-combustion processes, separation of CO_2 from H_2 is required for the stream leaving the water-shift reactor. This stream consists of 35–40% CO_2 at a temperature of 40–200 °C and typical pressures between 30 and 55 Bar. This stream may also contain small amounts of carbon monoxide and hydrogen sulfide. CO_2 removal from pre-combustion streams can be considered as an easier problem compared with the separation of post-combustion streams. This is due to the much higher concentration of carbon dioxide, much higher pressures involved and weak adsorption of hydrogen, compared to carbon dioxide, leading to high selectivity under a variety of conditions.

All simulations are run at the temperature of 313 K. We consider equimolar binary mixture of carbon dioxide and hydrogen, CO_2/H_2 = 40/60 case, and multi-component mixtures,

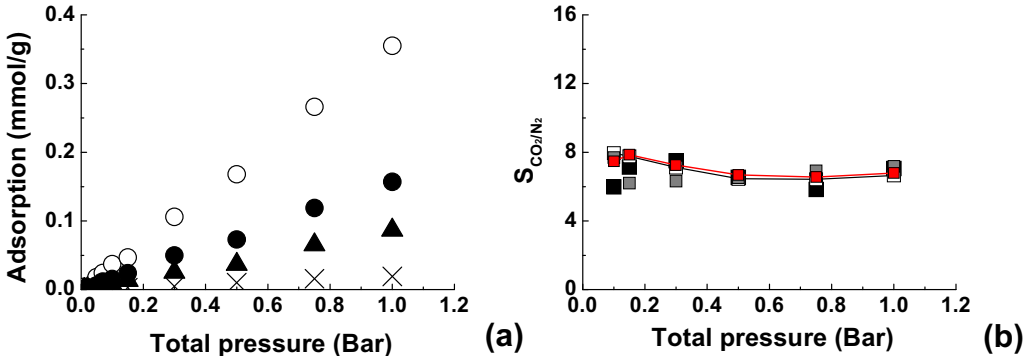

Fig. 12. (a) Excess adsorption isotherms for the mixture $CO_2/N_2/O_2/H_2O$ = 15/75/5/5. Filled circles are for CO_2, triangles are for N_2, cross shaped symbols are for O_2 as before, empty circles are for H_2O. (b) Carbon dioxide/nitrogen selectivities as a function of pressure for binary mixture CO_2/N_2 = 50/50 (black squares), binary mixture CO_2/N_2 = 10/90 (white squares and a black line), ternary mixture $CO_2/N_2/O_2$ = 15/80/5 (gray squares) and quaternary mixture $CO_2/N_2/O_2/H_2O$ = 15/75/5/5 (red squares and line). Lines are for eye guidance only. (A color version of this figure can be viewed online.)

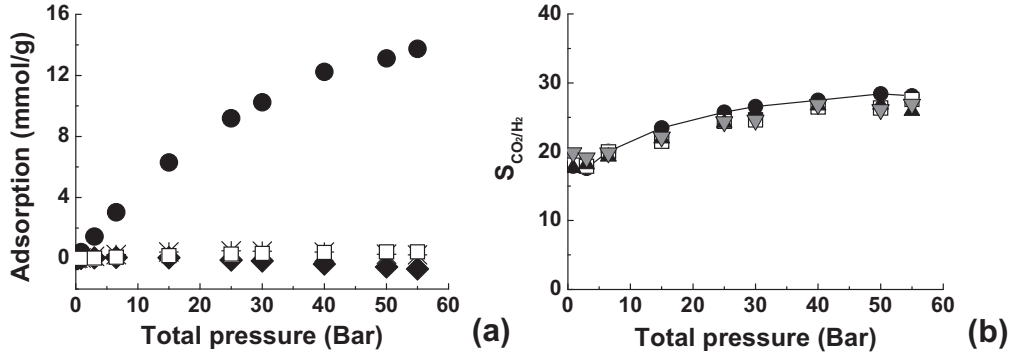

Fig. 13. (a) Excess adsorption isotherms for the mixture $CO_2/H_2/CO/H_2S$ = 38/60/1/1. Filled circles are for CO_2, diamonds are for H_2, stars are for CO, and empty squares are for H_2S. (b) Carbon dioxide/hydrogen selectivities as a function of pressure for binary mixture CO_2/H_2 = 50/50 (black circles and line), binary mixture CO_2/H_2 = 40/60 (white squares), ternary mixture $CO_2/H_2/H_2S$ = 39/60/1 (black triangles) and quaternary mixture $CO_2/H_2/H_2S/CO$ = 38/60/1/1 (gray reverse triangles). The line is for eye guidance only.

which include small amounts of H_2S and CO, specifically ternary mixture $CO_2/H_2/H_2S$ = 39/60/1 and quaternary mixture $CO_2/H_2/H_2S/CO$ = 38/60/1/1, respectively.

These results are summarized in Fig. 13. Firstly, as an example, panel (a) shows adsorption isotherms for the quaternary mixture $CO_2/H_2/CO/H_2S$ case. The excess adsorption for hydrogen is negative, and this has been observed in all mixtures under consideration in this section, starting from the binary equimolar case (all isotherms are reported in the SI file, Section 6, including data for an alternative model of hydrogen). This effect implies that the density of adsorbed hydrogen is lower than in the corresponding bulk mixture, due to weak interaction of hydrogen with the adsorbent, compared to other species; but it may also be related to the way accessible micropore volume is calculated in the computational porosimetry. In the SI file we also provide more detailed isotherms for carbon monoxide and hydrogen sulfide, using appropriate *y*-axis scale (Section 6).

The efficiency of the carbon dioxide removal is further assessed in Fig. 13(b), which shows carbon dioxide-hydrogen selectivities as a function of pressure for all cases. The lowest pressure considered is 0.85 Bar, which is consistent with the lower bound of 1–1.5 Bar generally reported for the PSA processes involving high pressure streams [12,114]. Similarly to the post-combustion case the selectivities are not particularly affected by the composition of the mixture, and the presence of the minor components in the stream does not have a major effect either. Also, the general trend is a slow increase in the separation factors with pressure until a plateau is reached. In all cases presented in Fig. 13(b) the selectivities start from values around 18 and reach values of about 25 (about 27 for the equimolar mixture); these results are consistent with the zero loading selectivity in the Henry's law regime, for which a value of 17.82 is obtained.

We also notice that in Fig. 13(b) selectivities show lower degree of scattering, compared to the results for the post-combustion separation; this is consistent with the error analysis for the selectivities in this case: for the mixture CO_2/H_2 = 40/60 error in selectivity is estimated at 14.4% at 0.85 Bar, 4.49% at 6.5 Bar and 2.7% at 55 Bar. This is a result of larger number of adsorbed molecules in the simulation cell at higher pressures and hence lower uncertainty in the adsorbed densities (including hydrogen).

Comparing these results with the recent comprehensive study by Herm et al. [31] on a number of materials we note that the selectivity values 18–27 for Maxsorb are low compared to record-setting zeolites and MOFs which can exhibit CO_2/H_2 selectivity in hundreds under the same conditions. However, the majority of MOFs in the study by Herm et al., have CO_2/H_2 selectivity comparable to Maxsorb, or lower [31]. Other activated carbons (JX101, BPL) exhibit comparable (somewhat higher) selectivity [31].

We now consider the effect of small amounts of water on the adsorption of a quaternary mixture. Fig. 14(a) shows excess adsorption isotherms, while Fig. 14(b) shows CO_2/H_2 selectivities for the quinary system $CO_2/H_2/CO/H_2S/H_2O$ = 38.8/59/1/1/0.2, together with the selectivities already shown in Fig. 13. The upper limit of the pressure is 36.6 Bar, beyond which water starts to condense in this mixture.

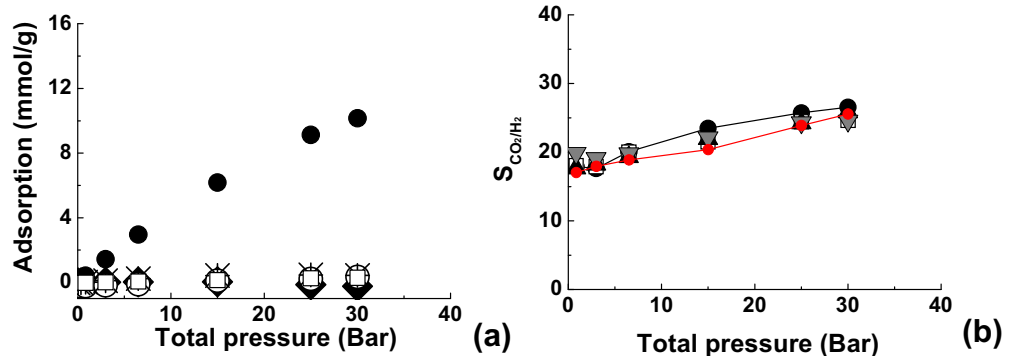

Fig. 14. (a) Excess adsorption isotherms for the mixture $CO_2/H_2/CO/H_2S/H_2O$ = 38.8/59/1/1/0.2 at 313 K. Filled circles are for CO_2, diamonds are for H_2, stars are for CO, empty squares are for H_2S, empty circles are for H_2O. (b) Carbon dioxide/hydrogen selectivities as a function of pressure for binary mixture CO_2/H_2 = 50/50 (black circles and line), binary mixture CO_2/H_2 = 40/60 (white squares), ternary mixture $CO_2/H_2/H_2S$ = 39/60/1 (black triangles), quaternary mixture $CO_2/H_2/H_2S/CO$ = 38/60/1/1 (reverse gray triangles), quinary mixture $CO_2/H_2/CO/H_2S/H_2O$ = 38.8/59/1/1/0.2 (red circles and line). Lines are for eye guidance only. (A color version of this figure can be viewed online.)

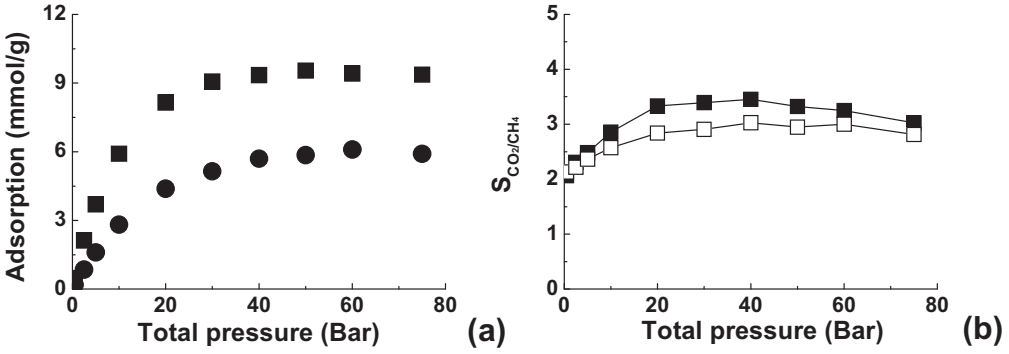

Fig. 15. (a) Excess adsorption isotherms for the mixture CO_2/CH_4 = 15/85 at 288 K. Circles are for CO_2, squares are for CH_4. (b) Carbon dioxide/methane selectivities as a function of pressure for binary mixture CO_2/CH_4 = 50/50 (black squares and line) and binary mixture CO_2/CH_4 = 15/85 (white squares and black line). Lines are for eye guidance only.

In the range of pressures we are considering water does not affect adsorption of other species. This is clear not only from Fig. 14(a), in which the isotherms are almost identical to the ones shown in Fig. 13(a), but also from Fig. 14(b), in which the selectivity for the system containing water exhibits values similar to those in the systems with no water. (A scaled-up version of Fig. 14 is provided in the SI file, Section 6).

The results shown in this section suggest that Maxsorb, despite not being the most selective among the materials presented in literature, is worth further investigation for applications in pre-combustion capture using adsorption. Again, selectivity is not the only parameter that needs to be considered in the development of an adsorption application. Other criteria such as high capacity at high pressure and the regenerability also need to be taken into account when assessing suitable materials. Maxsorb (and activated carbons in general) satisfies these criteria very well.

3.2.3. Sweetening of sour natural gas

In sweetening of sour natural gas the composition of the mixture and properties of the stream can vary substantially depending on the source of the fossil fuel. As a typical example we can consider a stream with molar percentage of CO_2 around 10–15% at temperatures between 10 and 40 °C and pressures >65 Bar [120].

In this case we focus on the main separation between carbon dioxide and methane and therefore consider binary mixtures only. Equimolar mixture of carbon dioxide and methane and a more realistic case of CO_2/CH_4 = 15/85 composition are investigated at a temperature of 288 K and pressures up to 75 Bar. Fig. 15(a) shows excess adsorption isotherms for the mixture CO_2/CH_4 = 15/85, while Fig. 15(b) shows selectivities for both mixtures as a function of pressure.

From this figure, Maxsorb is selective toward CO_2, however the values of selectivity are rather modest, between about 2 at lower pressures and not exceeding 4 at the maximum. In addition, selectivities for 15/85 mixture are uniformly shifted to lower values compared to the equimolar case. Zero loading selectivity in the Henry's law regime is calculated to be 2.04, consistent with the results shown in Fig. 15(b). The trend in the curves is similar to the trend observed in the case of pre-combustion, and the error in the selectivities ranges from 23% at 0.5 Bar, to 4.65% at 10 Bar, and down to 2.3% at 75 Bar.

Comparison with other literature data and experimental results is somewhat problematic in this case as not many studies consider the same conditions (in terms of pressure and temperature). At ambient pressures and temperatures, MOFs have selectivities between 3 and 30 [7], but these values are expected to drop substantially at higher temperatures and pressures.

Interestingly, a comparison with the study by Furmaniak and co-authors [38] shows that the selectivities we have predicted for Maxsorb correspond to the lower limit of the selectivities they calculated for oxidized virtual porous carbons. This aspect might need further investigation.

4. Conclusions

The purpose of this work was to investigate the behavior of high surface area activated carbons as adsorbents in CO_2 capture separations, using the model developed in our previous publication.

In particular, we have used GCMC simulations to study separation of multi-component mixtures involved in the pre- and post-combustion processes and in sweetening of sour natural gas, using realistic temperature and pressure conditions. For the cases of pre- and post-combustion we have also considered the presence of minor components in the mixture. These aspects are particularly important, since multi-component adsorption data is scarce and difficult to obtain experimentally.

Our approach is mostly based on the analysis of the simulated isotherms and focuses on the selectivity shown by the adsorbent for CO_2 over the other main component of each mixture. We are aware that more aspects should be considered for the evaluation of adsorbents in the context of CO_2 capture, but nonetheless selectivity gives a good initial indication of the efficiency of the separations.

Another aspect we take into account is the effect of water on the separations under consideration, given that humidity may have a great impact on the efficiency and the cost of the processes. For this, we first looked in detail into the behavior of water as an adsorptive, both as a single component and as a minor component in the presence of carbon dioxide. In either case the model confirms the previously reported behavior of water in activated carbons, i.e. the tendency to cluster and to interact with polar centers through hydrogen bonds. Analysis of the potential energy minima also revealed preferential locations of carbon dioxide and water molecules: Coulombic interactions strongly drive water molecules to form hydrogen bonds with the functional groups; carbon dioxide molecules, although also benefit from Coulombic interactions, prefer to be not at the edges of the platelets, but closer to the centers corresponding to the regions of the greatest dispersion interaction. This behavior also explains why, up to a certain concentration, water does not have a significant effect on the adsorption of carbon dioxide, given that the two species do not compete for the same sub-regions of the porous space.

Presence of the polar groups greatly affects the formation of the water clusters and adsorption of water. In the absence of the groups, the number of water clusters is diminished and the adsorption isotherm, including the location of capillary condensation, is shifted to much higher pressure. In our previous studies we showed that the type of the functional group does not have a significant impact in carbon dioxide and this current study explains why it is so: this interaction is not localized and the overall impact of the surface group is simply an increased polarity of the material. We speculate that adsorption of water, in contrast, should strongly depend on the type, location and accessibility of the surface groups. In fact these are additional parameters, that can be modulated in a model material to improve agreement between simulation results and experiments. This analysis applies to oxygen containing surface groups. Amine-functionalized carbons should be further investigated.

Extended to multicomponent systems, our results for Maxsorb carbon predict selectivities lower than those for most of the other materials in the context of post-combustion separation. For sweetening of sour natural gas the predicted selectivities are also quite low and in line with those for other activated carbons in general.

In the case of pre-combustion capture Maxsorb shows a reasonable selectivity performance, even though it is not the highest reported in literature. Furthermore, we show that presence of water has little effect on material performance under the conditions of interest. This result suggests that high surface area activated carbons might be worth further investigation for this type of separation, especially given that other parameters such as material cost and adsorption capacity would rank Maxsorb very favorably.

As shown in the SI file (Section 8) IAST provides an accurate description of adsorption of mixtures in application to all processes considered here, as long as the mixture under consideration does not include water.

Finally, the current study focuses exclusively on equilibrium adsorption properties. Kinetic aspects of adsorption also play an important role in the performance of the material in the actual separation process. Kinetics of carbon dioxide adsorption in activated carbons has been compared to that of zeolites (that is, adsorption is relatively fast) [5]. However an additional complexity may emerge in these systems from water clusters causing pore blocking effects and affecting structure accessibility for other molecules. This aspect requires further more systematic investigation and will be pursued in future studies.

Acknowledgments

We would like to thank Prof. Katsumi Kaneko for useful discussions and suggestions concerning adsorption of water in activated carbons. This work has made use of the resources provided by the Edinburgh Compute and Data Facility (ECDF) (http://www.ecdf.ed.ac.uk/). Financial support from EPSRC, Grant EP/GO62129/1 (IGSCC) is gratefully acknowledged.

Appendix A. Supplementary data

Supplementary data associated with this article can be found, in the online version, at http://dx.doi.org/10.1016/j.carbon.2015.06.056.

References

[1] D. Aaron, C. Tsouris, Separation of CO_2 from flue gas: a review, Sep. Sci. Technol. 40 (1–3) (2005) 321–348.
[2] A.D. Ebner, J.A. Ritter, State-of-the-art adsorption and membrane separation processes for carbon dioxide production from carbon dioxide emitting industries, Sep. Sci. Technol. 44 (6) (2009) 1273–1421.
[3] M.E. Boot-Handford, J.C. Abanades, E.J. Anthony, M.J. Blunt, S. Brandani, N. Mac Dowell, et al., Carbon capture and storage update, Energy Environ. Sci. 7 (1) (2014) 130–189.
[4] A.L. Chaffee, G.P. Knowles, Z. Liang, J. Zhang, P. Xiao, P.A. Webley, CO_2 capture by adsorption: materials and process development, Int. J. Greenhouse Gas Control 1 (1) (2007) 11–18.
[5] S. Choi, J.H. Drese, C.W. Jones, Adsorbent materials for carbon dioxide capture from large anthropogenic point sources, ChemSusChem 2 (9) (2009) 796–854.
[6] D.M. D'Alessandro, B. Smit, J.R. Long, Carbon dioxide capture: prospects for new materials, Angew. Chem. Int. Ed. 49 (35) (2010) 6058–6082.
[7] J.-R. Li, Y. Ma, M.C. McCarthy, J. Sculley, J. Yu, H.-K. Jeong, et al., Carbon dioxide capture-related gas adsorption and separation in metal-organic frameworks, Coord. Chem. Rev. 255 (15–16) (2011) 1791–1823.
[8] K. Sumida, D.L. Rogow, J.A. Mason, T.M. McDonald, E.D. Bloch, Z.R. Herm, et al., Carbon dioxide capture in metal-organic frameworks, Chem. Rev. 112 (2) (2011) 724–781.
[9] L. Espinal, B.D. Morreale, Materials challenges in carbon-mitigation technologies, MRS Bull. 37 (04) (2012) 431–438.
[10] T.C. Drage, C.E. Snape, L.A. Stevens, J. Wood, J. Wang, A.I. Cooper, et al., Materials challenges for the development of solid sorbents for post-combustion carbon capture, J. Mater. Chem. 22 (7) (2012) 2815–2823.
[11] B. Metz, O. Davidson, H.C. de Coninck, M. Loos, L.A. Meyer (Eds.), IPCC Special Report on Carbon Dioxide Capture and Storage. Prepared by Working Group III of the Intergovernmental Panel on Climate Change, Cambridge University Press, Cambridge, UK, 2005.
[12] L. Espinal, D.L. Poster, W. Wong-Ng, A.J. Allen, M.L. Green, Measurement, standards, and data needs for CO_2 capture materials: a critical review, Environ. Sci. Technol. 47 (21) (2013) 11960–11975.
[13] K.T. Chue, J.N. Kim, Y.J. Yoo, S.H. Cho, R.T. Yang, Comparison of activated carbon and zeolite 13X for CO_2 recovery from flue gas by pressure swing adsorption, Ind. Eng. Chem. Res. 34 (2) (1995) 591–598.
[14] S. Sircar, T.C. Golden, M.B. Rao, Activated carbon for gas separation and storage, Carbon 34 (1) (1996) 1–12.
[15] R.V. Siriwardane, M.-S. Shen, E.P. Fisher, J.A. Poston, Adsorption of CO_2 on molecular sieves and activated carbon, Energy Fuels 15 (2) (2001) 279–284.
[16] T.C. Drage, J.M. Blackman, C. Pevida, C.E. Snape, Evaluation of activated carbon adsorbents for CO_2 capture in gasification, Energy Fuels 23 (5) (2009) 2790–2796.
[17] H. Marsh, F. Rodríguez-Reinoso, Activated Carbon, Elsevier, 2006.
[18] T. Otowa, R. Tanibata, M. Itoh, Production and adsorption characteristics of MAXSORB: high-surface-area active carbon, Gas Sep. Purif. 7 (4) (1993) 241–245.

[19] D. Lozano-Castelló, D. Cazorla-Amorós, A. Linares-Solano, Powdered activated carbons and activated carbon fibers for methane storage: a comparative study, Energy Fuels 16 (5) (2002) 1321–1328.
[20] S. Himeno, T. Komatsu, S. Fujita, High-pressure adsorption equilibria of methane and carbon dioxide on several activated carbons, J. Chem. Eng. Data 50 (2) (2005) 369–376.
[21] M. Jordá-Beneyto, F. Suárez-García, D. Lozano-Castelló, D. Cazorla-Amorós, A. Linares-Solano, Hydrogen storage on chemically activated carbons and carbon nanomaterials at high pressures, Carbon 45 (2) (2007) 293–303.
[22] W.C. Xu, K. Takahashi, Y. Matsuo, Y. Hattori, M. Kumagai, S. Ishiyama, et al., Investigation of hydrogen storage capacity of various carbon materials, Int. J. Hydrogen Energy 32 (13) (2007) 2504–2512.
[23] Z. Yong, V. Mata, A. Rodrigues, Adsorption of carbon dioxide on chemically modified high surface area carbon-based adsorbents at high temperature, Adsorption 7 (1) (2001) 41–50.
[24] M.G. Plaza, C. Pevida, A. Arenillas, F. Rubiera, J.J. Pis, CO_2 capture by adsorption with nitrogen enriched carbons, Fuel 86 (14) (2007) 2204–2212.
[25] M. Sweatman, Improving the equilibrium performance of active carbons for separation processes by co-adsorption with low pressure solvent: application to carbon capture, Adsorption 17 (4) (2011) 723–737.
[26] F. Dreisbach, R. Staudt, J.U. Keller, High pressure adsorption data of methane, nitrogen, carbon dioxide and their binary and ternary mixtures on activated carbon, Adsorption 5 (3) (1999) 215–227.
[27] A. Busch, Y. Gensterblum, B.M. Krooss, Methane and CO_2 sorption and desorption measurements on dry Argonne premium coals: pure components and mixtures, Int. J. Coal Geol. 55 (2–4) (2003) 205–224.
[28] M. Sudibandriyo, Z. Pan, J.E. Fitzgerald, R.L. Robinson, K.A.M. Gasem, Adsorption of methane, nitrogen, carbon dioxide, and their binary mixtures on dry activated carbon at 318.2 K and pressures up to 13.6 MPa, Langmuir 19 (13) (2003) 5323–5331.
[29] S. Ottiger, R. Pini, G. Storti, M. Mazzotti, Competitive adsorption equilibria of CO_2 and CH_4 on a dry coal, Adsorption 14 (4–5) (2008) 539–556.
[30] J. Wu, L. Zhou, Y. Sun, W. Su, Y. Zhou, Measurement and prediction of adsorption equilibrium for a $H_2/N_2/CH_4/CO_2$ mixture, AIChE J. 53 (5) (2007) 1178–1191.
[31] Z.R. Herm, J.A. Swisher, B. Smit, R. Krishna, J.R. Long, Metal–organic frameworks as adsorbents for hydrogen purification and precombustion carbon dioxide capture, J. Am. Chem. Soc. 133 (15) (2011) 5664–5667.
[32] A.L. Myers, J.M. Prausnitz, Thermodynamics of mixed-gas adsorption, AIChE J. 11 (1) (1965) 121–127.
[33] R. Cracknell, D. Nicholson, S. Tennison, J. Bromhead, Adsorption and selectivity of carbon dioxide with methane and nitrogen in slit-shaped carbonaceous micropores: simulation and experiment, Adsorption 2 (3) (1996) 193–203.
[34] M. Heuchel, G.M. Davies, E. Buss, N.A. Seaton, Adsorption of carbon dioxide and methane and their mixtures on an activated carbon: simulation and experiment, Langmuir 15 (25) (1999) 8695–8705.
[35] M.B. Sweatman, N. Quirke, Modelling gas mixture adsorption in active carbons, Mol. Simul. 31 (9) (2005) 667–681.
[36] D. Cao, J. Wu, Modeling the selectivity of activated carbons for efficient separation of hydrogen and carbon dioxide, Carbon 43 (7) (2005) 1364–1370.
[37] P. Kowalczyk, P.A. Gauden, A.P. Terzyk, S. Furmaniak, P.J.F. Harris, Displacement of methane by coadsorbed carbon dioxide is facilitated in narrow carbon nanopores, J. Phys. Chem. C 116 (25) (2012) 13640–13649.
[38] S. Furmaniak, P. Kowalczyk, A.P. Terzyk, P.A. Gauden, P.J.F. Harris, Synergetic effect of carbon nanopore size and surface oxidation on CO_2 capture from CO_2/CH_4 mixtures, J. Colloid Interface Sci. 397 (2013) 144–153.
[39] X. Lu, D. Jin, S. Wei, M. Zhang, Q. Zhu, X. Shi, et al., Competitive adsorption of a binary CO_2–CH_4 mixture in nanoporous carbons: effects of edge-functionalization, Nanoscale 7 (2015) 1002–1012.
[40] K.V. Kumar, E.A. Müller, F. Rodríguez-Reinoso, Effect of pore morphology on the adsorption of methane/hydrogen mixtures on carbon micropores, J. Phys. Chem. C 116 (21) (2012) 11820–11829.
[41] V.K. Kumar, F. Rodríguez-Reinoso, Co-adsorption of N_2 in the presence of CH_4 within carbon nanospaces: evidence from molecular simulations, Nanotechnology 24 (3) (2013) 35401.
[42] J.K. Brennan, T.J. Bandosz, K.T. Thomson, K.E. Gubbins, Water in porous carbons, Colloids Surf. A 187–188 (2001) 539–568.
[43] E.A. Müller, L.F. Rull, L.F. Vega, K.E. Gubbins, Adsorption of water on activated carbons: a molecular simulation study, J. Phys. Chem. 100 (4) (1996) 1189–1196.
[44] I.I. Salame, T.J. Bandosz, Experimental study of water adsorption on activated carbons, Langmuir 15 (2) (1998) 587–593.
[45] I.I. Salame, A. Bagreev, T.J. Bandosz, Revisiting the effect of surface chemistry on adsorption of water on activated carbons, J. Phys. Chem. B 103 (19) (1999) 3877–3884.
[46] J. Choma, W. Burakiewicz-Mortka, M. Jaroniec, Z. Li, J. Klinik, Monitoring changes in surface and structural properties of porous carbons modified by different oxidizing agents, J. Colloid Interface Sci. 214 (2) (1999) 438–446.
[47] J. Miyawaki, T. Kanda, K. Kaneko, Hysteresis-associated pressure-shift-induced water adsorption in carbon micropores, Langmuir 17 (3) (2001) 664–669.
[48] M. Jorge, C. Schumacher, N.A. Seaton, Simulation study of the effect of the chemical heterogeneity of activated carbon on water adsorption, Langmuir 18 (24) (2002) 9296–9306.
[49] T. Ohba, K. Kaneko, Surface oxygen-dependent water cluster growth in carbon nanospaces with GCMC simulation-aided in situ SAXS, J. Phys. Chem. C 111 (17) (2007) 6207–6214.
[50] M. Nakamura, T. Ohba, P. Branton, H. Kanoh, K. Kaneko, Equilibration-time and pore-width dependent hysteresis of water adsorption isotherm on hydrophobic microporous carbons, Carbon 48 (1) (2010) 305–308.
[51] T.X. Nguyen, S.K. Bhatia, How water adsorbs in hydrophobic nanospaces, J. Phys. Chem. C 115 (33) (2011) 16606–16612.
[52] T.X. Nguyen, S.K. Bhatia, Some anomalies in the self-diffusion of water in disordered carbons, J. Phys. Chem. C 116 (5) (2012) 3667–3676.
[53] Y. Liu, J. Wilcox, Molecular simulation studies of CO_2 adsorption by carbon model compounds for carbon capture and sequestration applications, Environ. Sci. Technol. 47 (2013) 95–101.
[54] J.K. Brennan, K.T. Thomson, K.E. Gubbins, Adsorption of water in activated carbons: effects of pore blocking and connectivity, Langmuir 18 (14) (2002) 5438–5447.
[55] J.C. Liu, P.A. Monson, Monte Carlo simulation study of water adsorption in activated carbon, Ind. Eng. Chem. Res. 45 (16) (2006) 5649–5656.
[56] T. Horikawa, N. Sakao, D.D. Do, Effects of temperature on water adsorption on controlled microporous and mesoporous carbonaceous solids, Carbon 56 (2013) 183–192.
[57] R. Wang, Y. Amano, M. Machida, Surface properties and water vapor adsorption–desorption characteristics of bamboo-based activated carbon, J. Anal. Appl. Pyrolysis 104 (2013) 667–674.
[58] E.I. Segarra, E.D. Glandt, Model microporous carbons: microstructure, surface polarity and gas adsorption, Chem. Eng. Sci. 49 (17) (1994) 2953–2965.
[59] D.D. Do, H.D. Do, A model for water adsorption in activated carbon, Carbon 38 (5) (2000) 767–773.
[60] D.D. Do, S. Junpirom, H.D. Do, A new adsorption–desorption model for water adsorption in activated carbon, Carbon 47 (6) (2009) 1466–1473.
[61] T. Horikawa, T. Sekida, Ji Hayashi, M. Katoh, D.D. Do, A new adsorption–desorption model for water adsorption in porous carbons, Carbon 49 (2) (2011) 416–424.
[62] L. Cossarutto, T. Zimny, J. Kaczmarczyk, T. Siemieniewska, J. Bimer, J.V. Weber, Transport and sorption of water vapour in activated carbons, Carbon 39 (15) (2001) 2339–2346.
[63] S. Furmaniak, P.A. Gauden, A.P. Terzyk, G. Rychlicki, R.P. Wesołowski, P. Kowalczyk, Heterogeneous Do–Do model of water adsorption on carbons, J. Colloid Interface Sci. 290 (1) (2005) 1–13.
[64] S. Lagorsse, M.C. Campo, F.D. Magalhães, A. Mendes, Water adsorption on carbon molecular sieve membranes: experimental data and isotherm model, Carbon 43 (13) (2005) 2769–2779.
[65] M. Neitsch, W. Heschel, M. Suckow, Water vapor adsorption by activated carbon: a modification to the isotherm model of Do and Do, Carbon 39 (9) (2001) 1437–1438.
[66] B.M. Krooss, F. van Bergen, Y. Gensterblum, N. Siemons, H.J.M. Pagnier, P. David, High-pressure methane and carbon dioxide adsorption on dry and moisture-equilibrated Pennsylvanian coals, Int. J. Coal Geol. 51 (2) (2002) 69–92.
[67] Y. Wang, Y. Zhou, C. Liu, L. Zhou, Comparative studies of CO_2 and CH_4 sorption on activated carbon in presence of water, Colloids Surf. A 322 (1–3) (2008) 14–18.
[68] Y. Sun, Y. Wang, Y. Zhang, Y. Zhou, L. Zhou, CO_2 sorption in activated carbon in the presence of water, Chem. Phys. Lett. 437 (1–3) (2007) 14–16.
[69] Y. Sun, Q. Xue, Y. Zhou, L. Zhou, Sorption equilibria of CO_2/CH_4 mixture on activated carbon in presence of water, J. Colloid Interface Sci. 322 (1) (2008) 22–26.
[70] P. Billemont, B. Coasne, G. De Weireld, An experimental and molecular simulation study of the adsorption of carbon dioxide and methane in nanoporous carbons in the presence of water, Langmuir 27 (3) (2010) 1015–1024.
[71] P. Billemont, B. Coasne, G. De Weireld, Adsorption of carbon dioxide, methane, and their mixtures in porous carbons: effect of surface chemistry, water content, and pore disorder, Langmuir 29 (10) (2013) 3328–3338.
[72] J.E. Fitzgerald, Z. Pan, M. Sudibandriyo, J.R.L. Robinson, K.A.M. Gasem, S. Reeves, Adsorption of methane, nitrogen, carbon dioxide and their mixtures on wet Tiffany coal, Fuel 84 (18) (2005) 2351–2363.
[73] D. Xu, P. Xiao, J. Zhang, G. Li, G. Xiao, P.A. Webley, et al., Effects of water vapour on CO_2 capture with vacuum swing adsorption using activated carbon, Chem. Eng. J. 230 (2013) 64–72.
[74] D. Xu, J. Zhang, G. Li, P. Xiao, P. Webley, Y.-C. Zhai, Effect of water vapor from power station flue gas on CO_2 capture by vacuum swing adsorption with activated carbon, J. Fuel Chem. Technol. 39 (3) (2011) 169–174.
[75] E. Di Biase, L. Sarkisov, Systematic development of predictive molecular models of high surface area activated carbons for adsorption applications, Carbon 64 (2013) 262–280.
[76] T. Otowa, Y. Nojima, T. Miyazaki, Development of KOH activated high surface area carbon and its application to drinking water purification, Carbon 35 (9) (1997) 1315–1319.
[77] Y. Huang, F.S. Cannon, J.K. Watson, B. Reznik, J.P. Mathews, Activated carbon efficient atomistic model construction that depicts experimentally-determined characteristics, Carbon 83 (2015) 1–14.
[78] T.X. Nguyen, N. Cohaut, J.-S. Bae, S.K. Bhatia, New method for atomistic modeling of the microstructure of activated carbons using hybrid reverse Monte Carlo simulation, Langmuir 24 (15) (2008) 7912–7922.

[79] J.C. Palmer, J.K. Brennan, M.M. Hurley, A. Balboa, K.E. Gubbins, Detailed structural models for activated carbons from molecular simulation, Carbon 47 (12) (2009) 2904–2913.
[80] A.H. Farmahini, G. Opletal, S.K. Bhatia, Structural modelling of silicon carbide-derived nanoporous carbon by hybrid reverse Monte Carlo simulation, J. Phys. Chem. C 117 (27) (2013) 14081–14094.
[81] L. Sarkisov, A. Harrison, Computational structure characterisation tools in application to ordered and disordered porous materials, Mol. Simul. 37 (15) (2011) 1248–1257.
[82] L. Sarkisov, Toward rational design of metal-organic frameworks for sensing applications: efficient calculation of adsorption characteristics in zero loading regime, J. Phys. Chem. C 116 (4) (2012) 3025–3033.
[83] A. Gupta, S. Chempath, M.J. Sanborn, L.A. Clark, R.Q. Snurr, Object-oriented programming paradigms for molecular modeling, Mol. Simul. 29 (1) (2003) 29–46.
[84] O. Talu, A.L. Myers, Molecular simulation of adsorption: Gibbs dividing surface and comparison with experiment, AlChE J. 47 (5) (2001) 1160–1168.
[85] C.M. Tenney, C.M. Lastoskie, Molecular simulation of carbon dioxide in chemically and structurally heterogeneous porous carbons, Environ. Prog. 25 (4) (2006) 343.
[86] W.A. Steele, The interaction of rare gas atoms with graphitized carbon black, J. Phys. Chem. 82 (7) (1978) 817–821.
[87] S.J. Weiner, P.A. Kollman, D.A. Case, U.C. Singh, C. Ghio, G. Alagona, et al., A new force field for molecular mechanical simulation of nucleic acids and proteins, J. Am. Chem. Soc. 106 (3) (1984) 765–784.
[88] W.L. Jorgensen, J.D. Madura, C.J. Swenson, Optimized intermolecular potential functions for liquid hydrocarbons, J. Am. Chem. Soc. 106 (22) (1984) 6638–6646.
[89] M. Freindorf, J. Gao, Optimization of the Lennard-Jones parameters for a combined ab initio quantum mechanical and molecular mechanical potential using the 3–21G basis set, J. Comput. Chem. 17 (4) (1996) 386–395.
[90] W.L. Jorgensen, D.S. Maxwell, J. Tirado-Rives, Development and testing of the OPLS all-atom force field on conformational energetics and properties of organic liquids, J. Am. Chem. Soc. 118 (45) (1996) 11225–11236.
[91] D.B. Axel, A new mixing of Hartree-Fock and local density-functional theories, J. Chem. Phys. 98 (2) (1993) 1372–1377.
[92] C.M. Breneman, K.B. Wiberg, Determining atom-centered monopoles from molecular electrostatic potentials. The need for high sampling density in formamide conformational analysis, J. Comput. Chem. 11 (3) (1990) 361–373.
[93] M.J.T. Frisch, G.W. Trucks, H.B. Schlegel, G.E. Scuseria, M.A. Robb, J.R. Cheeseman et al., Gaussian 09, Revision A.1., 2009.
[94] M.G. Martin, J.I. Siepmann, Transferable potentials for phase equilibria. 1. United-atom description of n-alkanes, J. Phys. Chem. B 102 (14) (1998) 2569–2577.
[95] B. Chen, J.J. Potoff, J.I. Siepmann, Monte Carlo calculations for alcohols and their mixtures with alkanes. transferable potentials for phase equilibria. 5. United-atom description of primary, secondary, and tertiary alcohols, J. Phys. Chem. B 105 (15) (2001) 3093–3104.
[96] L. Zhang, J.I. Siepmann, Direct calculation of Henry's law constants from Gibbs ensemble Monte Carlo simulations: nitrogen, oxygen, carbon dioxide and methane in ethanol, Theor. Chem. Acc. 115 (5) (2006) 391–397.
[97] G. Kamath, N. Lubna, J.J. Potoff, Effect of partial charge parametrization on the fluid phase behavior of hydrogen sulfide, J. Chem. Phys. 123 (12) (2005). Sep.
[98] V. Buch, Path integral simulations of mixed *para*-D_2 and *ortho*-D_2 clusters: the orientational effects, J. Chem. Phys. 100 (10) (1994) 7610–7629.
[99] M.B. Sweatman, N. Quirke, Modelling gas adsorption in slit-pores using Monte Carlo simulation, Mol. Simul. 27 (5–6) (2001) 295–321.
[100] W.L. Jorgensen, J. Chandrasekhar, J.D. Madura, R.W. Impey, M.L. Klein, Comparison of simple potential functions for simulating liquid water, J. Chem. Phys. 79 (2) (1983) 926–935.
[101] C.J. Fennel, D. Gezelter, Is the Ewald summation still necessary? Pairwise alternatives to the accepted standard for long-range electrostatics, J. Chem. Phys. 124 (2006) 234104.
[102] P.P. Ewald, Die Berechnung optischer und elektrostatischer Gitterpotentiale, Ann. Phys. 369 (3) (1921) 253–287.
[103] A.-M. Banu, D. Friedrich, S. Brandani, T. Düren, A multiscale study of MOFs as adsorbents in H_2 PSA purification, Ind. Eng. Chem. Res. 52 (29) (2013) 9946–9957.
[104] M.M.F. Hasan, R.C. Baliban, J.A. Elia, C.A. Floudas, Modeling, simulation, and optimization of postcombustion CO_2 capture for variable feed concentration and flow rate. 2. Pressure swing adsorption and vacuum swing adsorption processes, Ind. Eng. Chem. Res. 51 (48) (2012) 15665–15682.
[105] D.L. Carlile, D.K. Friday, Chemical Research D, Center E. 1,1,2-trichloro, 1,2,2-trifluoroethane (CFC-113) and Water Isotherm Measurements on Impregnated and Unimpregnated Activated Carbons: Chemical Research, Development & Engineering Center, 1992.
[106] R.F. Cracknell, D. Nicholson, N.G. Parsonage, H. Evans, Rotational insertion bias: a novel method for simulating dense phases of structured particles, with particular application to water, Mol. Phys. 71 (5) (1990) 931–943.
[107] J. Rouquerol, F. Rouquerol, K.S.W. Sing, Adsorption by Powders and Porous Solids: Principles, Methodology and Applications, Academic Press, 1999.
[108] S.Y. Qi, K.J. Hay, M.J. Rood, M.P. Cal, Equilibrium and heat of adsorption for water vapor and activated carbon, J. Environ. Eng. 126 (3) (2000) 267–271.
[109] A.K. Soper, The radial distribution functions of water and ice from 220 to 673 K and at pressures up to 400 MPa, Chem. Phys. 258 (2–3) (2000) 121–137.
[110] C. Vega, C. McBride, E. Sanz, J.L.F. Abascal, Radial distribution functions and densities for the SPC/E, TIP4P and TIP5P models for liquid water and ices I-h, I-c, II, III, IV, V, VI, VII, VIII, IX, XI and XII, PCCP 7 (7) (2005) 1450–1456.
[111] R. Ishii, S. Okazaki, I. Okada, M. Furusaka, N. Watanabe, M. Misawa, et al., Density dependence of structure of supercritical carbon dioxide along an isotherm, J. Chem. Phys. 105 (16) (1996) 7011–7021.
[112] A. Zhu, X. Zhang, Q. Liu, Q. Zhang, A fully flexible potential model for carbon dioxide, Chin. J. Chem. Eng. 17 (2) (2009) 268–272.
[113] P. Kluson, S.J. Scaife, Microporous adsorbents for a selective separation of carbon dioxide from mixtures with methane and nitrogen, Chem. Biochem. Eng. Q 16 (3) (2002) 97–103.
[114] Y.-S. Bae, R.Q. Snurr, Development and evaluation of porous materials for carbon dioxide separation and capture, Angew. Chem. Int. Ed. 50 (49) (2011) 11586–11596.
[115] J.-H. Park, J.-N. Kim, S.-H. Cho, J.-D. Kim, R.T. Yang, Adsorber dynamics and optimal design of layered beds for multicomponent gas adsorption, Chem. Eng. Sci. 53 (23) (1998) 3951–3963.
[116] S. Cavenati, C.A. Grande, A.E. Rodrigues, Adsorption equilibrium of methane, carbon dioxide, and nitrogen on zeolite 13X at high pressures, J. Chem. Eng. Data 49 (4) (2004) 1095–1101.
[117] Y.-S. Bae, O.K. Farha, J.T. Hupp, R.Q. Snurr, Enhancement of CO_2/N_2 selectivity in a metal-organic framework by cavity modification, J. Mater. Chem. 19 (15) (2009) 2131–2134.
[118] R. Banerjee, H. Furukawa, D. Britt, C. Knobler, M. O'Keeffe, O.M. Yaghi, Control of pore size and functionality in isoreticular zeolitic imidazolate frameworks and their carbon dioxide selective capture properties, J. Am. Chem. Soc. 131 (11) (2009) 3875–3877.
[119] Y.-S. Bae, A.M. Spokoyny, O.K. Farha, R.Q. Snurr, J.T. Hupp, C.A. Mirkin, Separation of gas mixtures using Co(ii) carborane-based porous coordination polymers, Chem. Commun. 46 (20) (2010) 3478–3480.
[120] T.V. Alonso, High efficiency on CO2 removal in natural gas with UCARSOLTM solvents, in: Rio Oil & Gas Expo and Conference Proceedings, Rio de Janeiro, Brazil, 2010.